

Phase transition in magic with random quantum circuits

Received: 6 June 2023

Accepted: 12 August 2024

Published online: 23 September 2024

 Check for updates

Pradeep Niroula ^{1,2}✉, Christopher David White¹, Qingfeng Wang ^{2,3},
Sonika Johri⁴, Daiwei Zhu ⁴, Christopher Monroe ^{1,2,4,5}, Crystal Noel ⁵ &
Michael J. Gullans ¹✉

Magic is a property of quantum states that enables universal fault-tolerant quantum computing using simple sets of gate operations. Understanding the mechanisms by which magic is created or destroyed is, therefore, a crucial step towards efficient and practical fault-tolerant computation. Many proposals for error correction in quantum computing make use of so-called stabilizer codes, which use multiqubit measurements to detect deviations from logical qubit states. Here we observe that a random stabilizer code subject to coherent errors exhibits a phase transition in magic, which we characterize through analytical, numerical and experimental probes. Below a critical error rate, stabilizer measurements remove the accumulated magic in the circuit, effectively protecting against coherent errors; above the critical error rate measurements concentrate magic. A better understanding of this behaviour in the resource theory of magic could help to identify the origins of quantum speedup and lead to methods for more efficient magic state generation.

A central goal in physics and computer science is to understand the origins of possible computational speedups of quantum information processors over their classical counterparts. Entanglement is a central resource for fault-tolerant quantum computing, but it is not necessarily sufficient to realize computational speedups. The notion of entanglement must be extended to distinguish between the production of ‘easy’ and ‘hard’ quantum states by fault-tolerant operations. Notably, even when the quantum state of the processor is highly entangled, computations consisting of only Clifford gates—a finite, non-universal subgroup of the unitary group—applied to stabilizer states, or eigenstates of Pauli operators, can be efficiently simulated on classical computers^{1,2}. Non-stabilizer input states or non-Clifford gates, by contrast, are believed to be exponentially difficult to simulate on classical computers^{3,4}. On quantum computers non-Clifford gates are easy; however, in the context of error-corrected quantum computer, these states and operations still require costly magic state distillation or other gate-intensive protocols^{5–8}.

A resource theory of stabilizer computation has emerged⁹ to study this division between easy (Clifford) and hard (non-Clifford) gates. In this theory, magic is the resource that enables universal quantum computation; the amount of magic in a state determines how useful it is as a non-stabilizer input state in fault-tolerant synthesis of non-Clifford operations. Magic has been used to bound quantum complexities¹⁰ and to constrain tensor network models of AdS-CFT¹¹. Magic-generating non-Clifford operations have also been shown to be necessary for simulating quantum chaos¹². Understanding the mechanisms by which magic can be generated or suppressed in a quantum circuit is, therefore, necessary not only to accelerate progress towards universal quantum computing but also to understand the limits in which quantum computations become classically accessible.

A related aspect of quantum entanglement is its behaviour in monitored quantum circuits, such as measurement-induced entanglement phase transitions^{13,14}. Monitored quantum circuits consist of local gates (or time evolution), interspersed with some rate or density of projective

¹Joint Center for Quantum Information and Computer Science, University of Maryland and NIST, College Park, MD, USA. ²Joint Quantum Institute, University of Maryland and NIST, College Park, MD, USA. ³Chemical Physics Program and Institute for Physical Science and Technology, University of Maryland, College Park, MD, USA. ⁴IonQ, Inc., College Park, MD, USA. ⁵Duke Quantum Center, Department of Electrical & Computer Engineering and Department of Physics, Duke University, Durham, NC, USA. ✉e-mail: pniroula@umd.edu; mgullans@umd.edu

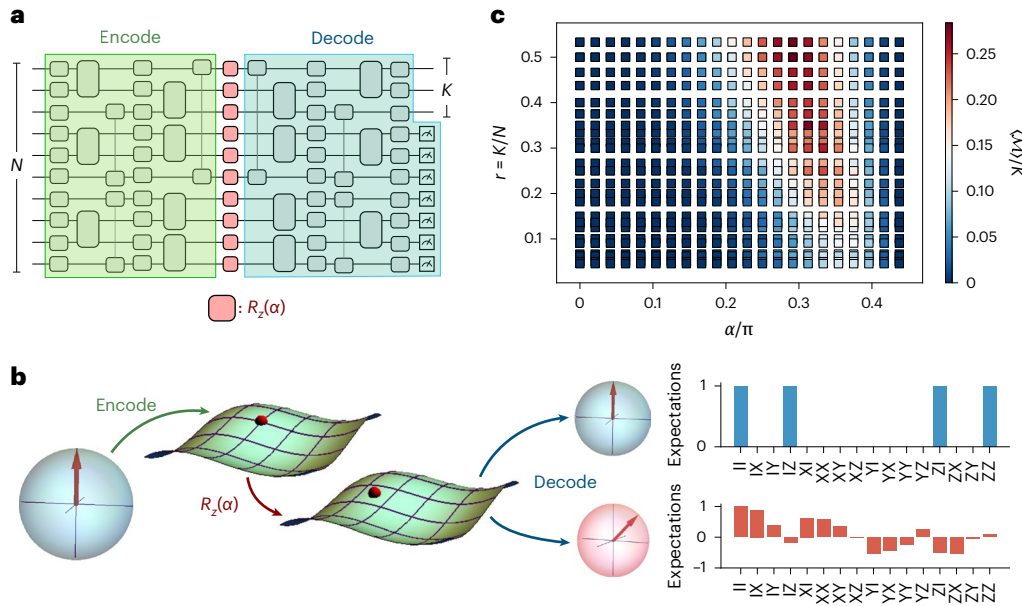


Fig. 1 | Model and phase diagram. **a**, The model. The qubits start in an all-zero state, corresponding to a logical 0 state. We apply a random Clifford encoding circuit (green), controlled ‘error’ unitaries (red), and the conjugate of the encoding circuit (blue). **b**, A schematic illustration of how magic is created or destroyed in our model. The encoding step acting on an input stabilizer state (represented by a blue Bloch sphere) produces a highly entangled stabilizer state in the many-qubit Hilbert space. Coherent rotations move the state off the grid of stabilizer states. The decoding step either snaps the state back to the grid of

stabilizer states or pushes the state away from that grid. The final state is either a multiqubit stabilizer state, represented by a Bloch sphere shaded blue, or a magical state, represented by a Bloch sphere shaded red. The Pauli expectations of the resulting stabilizer (magical) state are shown as histograms shaded blue (red). **c**, Phase diagram for constant-rate codes. The colour bar represents the magic density at a particular code rate r , given by the ratio of logical qubits K and total number of qubits N , and the error rate, defined to be the angle of coherent rotation, α .

measurements. The simplest example of a monitored quantum circuit is the error correcting code: the state undergoes a series of entangling ‘encoding’ unitaries, followed by projective syndrome measurement and final logical ‘decoding’ unitaries¹⁵. In general, monitored quantum circuits can display a measurement-induced phase transition in entanglement. These systems display evidence of a complicated phase diagram determined by the details of the circuit^{16–18}, and have connections to percolation theory^{13,19}, the theory of stabilizer codes²⁰ and statistical mechanics models^{21–24}. Such hybrid circuits have also been shown to exhibit related phase transitions beyond entanglement²⁵.

In this paper, we show that measurement-induced phase transitions of entanglement can be extended to magic, and we study the transition experimentally. A quantum error correcting code subject to coherent errors displays a phase transition in the magic as a function of the number of logical qubits (which in our model sets the measurement rate) or the error rate. In the magic phase transition, syndrome measurements, which can destroy magic, compete with errors, which can create magic, just as local dynamics and local measurement compete in the entanglement transition. For large error rate or infrequent measurements, the encoded state has extensive magic, whereas for low error rate or frequent measurements, the encoded state has nearly zero magic; the two regimes are separated by a phase transition. A brief overview of our set-up is sketched in Fig. 1a,b and the resulting phase diagram is given in Fig. 1c. We also introduce a new measure of magic, the basis-minimized measurement entropy. We measure this quantity and another known measure of magic, the stabilizer Rényi entropy²⁶, in classical simulations, analytical calculations and experiments on IonQ’s Aria trapped-ion quantum computer. The magic phase transition is visible as a finite-size scaling collapse in these measures.

Model

We study magic in random Clifford codes. The initial state is a product state of N qubits, $|0\rangle^{\otimes N}$. A randomly drawn Clifford circuit C is applied to this state. This Clifford circuit maps the initial state to the logical

space of a random Clifford code; such codes are known to make high-performing error correcting codes²⁷. After encoding circuit C , a single-qubit rotation $R_z(\alpha) = \exp(-i\sigma_z\alpha/2)$, with σ_z being the Pauli Z operator, is applied to each qubit. This ‘noise layer’ models coherent noise and takes the quantum state away from the codespace of the Clifford code. We call α the error rate. The noise layer is followed by C^\dagger , the conjugate of the encoding circuit. Finally, $N - K$ qubits are measured in the computational basis, leaving a logical state with K qubits. These $N - K$ measurements are syndrome measurements for the Clifford code.

The encoding Clifford circuits are generated by interweaving d layers of single-qubit unitaries and d layers of two-qubit Clifford unitaries (Fig. 1a). The odd layers are single-qubit gates sampled uniformly from the 24 elements of the single-qubit Clifford group. The even layers consist of fixed-angle $(\pi/2)$ entangling Mølmer–Sørensen gates, defined as $MS(\pi/2) = e^{i\pi\sigma_x\sigma_x/4}$, applied to $N/2$ randomly chosen disjoint pairs. The decoding circuit is the inverse of the encoder. We take $d = N$ in numerical calculations and $d = N/2$ in the experiment to reduce the effects of noise. Circuits with $d = N/2$ have a behaviour similar to that with depth $d = N$. In Supplementary Information Section E, we present numerical data on $d = N/2$ and $d = 2N$ circuits.

Figure 1b illustrates how magic is created or destroyed in our model. The state begins as a logical stabilizer state. The Bloch sphere, shaded blue, represents a multiqubit stabilizer state. The encoding step maps the state to a stabilizer state in a many-qubit Hilbert space, and error moves the state off the grid of stabilizer states. The decoding (conjugate of the encoding operator together with syndrome measurements) step either snaps the state back to the grid of stabilizer states or pushes the state away from that grid; in either case it projects the state back to the logical space. The final state is either a multiqubit stabilizer state, represented by a Bloch sphere shaded blue, or a magical state, represented by a Bloch sphere shaded red. The stabilizerness of a state is visible in the Pauli expectations. For a stabilizer state, the distribution of expectations is concentrated among the stabilizing Paulis, as shown in the histogram shaded blue for a representative two-qubit

stabilizer state. For a Haar state, the distribution has support over all Paulis, as shown in the histogram shaded red for a representative two-qubit Haar state.

We study this transition for two different code rates. (The code rate is the ratio of the number of logical qubits to underlying physical qubits.) The first case, which we refer to as ‘vanishing rate’, has only one logical qubit, so the code rate $r = 1/N$ tends to be zero for large N . The second case uses constant-rate codes with the scaling $K = rN$ logical qubits for a fixed code rate r .

Quantifying magic

Any measure of magic for pure states is a function of quantum states, which is zero for stabilizer states and non-increasing under Clifford unitaries. Measures of magic can also be used to quantify the non-Clifford resources required to prepare a state, and how useful it can be in synthesizing non-Clifford gates by means of magic state distillation and injection. We consider two measures of magic: the second stabilizer Rényi entropy (SSRE)^{26,28} and the basis-minimized measurement entropy.

The SSRE measures how spread out the state’s density matrix is when expanded in the basis of Pauli operators. A key property of stabilizer states is that they are the common eigenstate of a maximal set of mutually commuting Pauli operators²⁹. As a result, the stabilizer state’s density matrix is only supported on those operators, so it is maximally concentrated and the SSRE is zero. A Haar state on N qubits, by contrast, has approximately equal weight on all Pauli operators, so it is nearly maximally spread out and the SSRE, defined as $M_2(\rho) = -\log \frac{1}{2^N} \sum_{P \in \mathcal{P}} \text{Tr}(\rho P)^2$ for a density matrix ρ on N qubits with a sum over all Pauli operators P in the Pauli group \mathcal{P} , is proportional to N . The histograms in Fig. 1b illustrate the distribution of Pauli expectations for these two cases.

We also consider a second measure of magic, which we call basis-minimized measurement entropy, defined as the entropy of the Born probability distribution of measurement outcomes, minimized over the finite set of possible stabilizer measurement bases. For example, consider a two-qubit stabilizer state $|00\rangle$ that we can measure in arbitrary length-two Pauli bases, including X_1X_2 and Z_1Z_2 . Measuring X_1X_2 will result in a Born probability distribution of four equally possible measurement outcomes $|\pm\pm\rangle$, giving an entropy of two. On the other hand, measuring in Z_1Z_2 results in only one outcome $|00\rangle$, giving an entropy of zero. Minimizing the entropy over all possible measured bases, the resulting basis-minimized measurement entropy is zero in this case. We wish to compute this basis-minimized measurement entropy for the resulting logical state in our model—that is, the state on the logical qubits after encoding, noise, application of the inverse of the encoding circuit and syndrome measurement. In Supplementary Information Section A, we show that the basis-minimized entropy is a good measure of non-stabilizerness for pure states. It is zero for a stabilizer state, is non-increasing under Clifford unitaries and is subadditive for product states, that is, $f(\sigma \otimes \rho) \leq f(\sigma) + f(\rho)$.

The basis-minimized measurement entropy of the logical state depends on the syndrome outcome. Averaging the entropy of the logical state over all syndromes s gives us the basis-minimized classical conditional entropy $\min_B S_{l_b|s} = \min_B (S_{l_b,s} - S_s)$, where S_s is the entropy of the distribution of syndromes, B is a stabilizer basis for the logical Hilbert space and l_b is the outcome of measurement in stabilizer basis B . Furthermore, the conditional entropy without any basis minimization serves as a good upper bound in the non-magical phase. Below the code’s error-correction threshold, the logical state is close to the initial computational basis state, so we expect the optimal basis to be the computational basis. So, for small α in our model, we expect the optimal basis to be the computational basis, and the conditional entropy is close to its optimal value (after basis minimization). Furthermore, the Rényi analogue of the conditional entropy, $S_{l_b,s}^{(2)} - S_s^{(2)}$ where $S_X^{(2)} = -\log \sum_{x \in \mathcal{X}} p_x^2$ is the Rényi entropy of distribution \mathcal{X} , is analytically

approachable. We compute the conditional entropy by classical simulation and experiment, and the Rényi analogue by experiment and analytical calculations.

The conditional entropy of the logical state quantifies the uncertainty in the logical space given a syndrome measurement, and it directly bounds the ability of a decoder to recover encoded classical information from measurements of the logical qubits (Supplementary Information Section C). A decoder is a syndrome-dependent operation that corrects logical errors corresponding to the syndrome measured. Whereas the basis-minimized conditional entropy measures the minimal uncertainty over all possible Clifford decoding operations, the conditional entropy without basis minimization limits the decoder to measurements in the computational basis.

In our experiment, we measured these measures of magic as a function of the error rate α , tuning it from 0 to $\pi/2$. At zero error ($\alpha = 0$) and maximal error ($\alpha = \pi/2$), both measures are identically zero, because in each case the state is a stabilizer state. When $\alpha = 0$, the noise layer acts as the identity operator, the encoding circuit C is cancelled by the following C^\dagger and the final state is the same as the input stabilizer state. When $\alpha = \pi/2$, the error operator $e^{-i\alpha Z/2}$ is itself a Clifford gate, so the magic is likewise zero.

Magic in the vanishing-rate code

First, we discuss the vanishing-rate case with a single logical qubit. Between the two special Clifford points $\alpha = 0, \pi/2$ the logical qubit has finite magic according to SSRE, with a peak at a distance $\propto 1/\sqrt{N}$ away from the Clifford point $\alpha = \pi/2$ point (Fig. 2b). At large N , the Clifford point, therefore, becomes a singularity. We can understand the square-root scaling by perturbing around the Clifford point $\alpha = \pi/2$. At the Clifford point, the logical state is not magical because it is an equal superposition over states corresponding to that syndrome. Away from the Clifford point, the logical state becomes magical to the extent that the amplitudes in the superposition are no longer equal. If exactly two errors give rise to each syndrome and the two errors corresponding to the measured syndrome have weights n_a and n_b , then the ratio of amplitudes is $[\tan(\pi/2 - \alpha)]^{(n_a - n_b)} \approx (\pi/2 - \alpha)(n_a - n_b)$ and the SSRE is $\mathcal{M}_2 \approx (\pi/2 - \alpha)^2 (n_a - n_b)^2$ (Supplementary Information Section F). Figure 2a shows the SSRE for classical simulations of circuits; the distribution is sharply peaked near this prediction. Because the error weights n_a and n_b controlling the SSRE are drawn from a binomial distribution, averaging over syndromes gives $\mathcal{M}_2 \propto N(\pi/2 - \alpha)^2 = f(\pi/2 - \alpha)\sqrt{N}$. (See Supplementary Information D for details.) Figure 2b shows the syndrome- and circuit-averaged SSRE as a function of error angle α . Figure 2c shows the same quantity for experiments (see below). Both show the predicted square-root scaling $\langle \mathcal{M}_2 \rangle = f(\pi/2 - \alpha)\sqrt{N}$. It is interesting to note that some of the same behaviour occurs in the case of zero-rate surface codes³⁰. In that case, the breakdown of the code and generation of magic in the logical qubit occurs at a threshold value below the Clifford point and can be understood through mappings to Anderson localization³¹. Here, we focus on random stabilizer codes for their conceptual simplicity and natural generalization to a finite density of logical qubits, as considered in the next section.

Experiment

We perform our experiments on IonQ’s Aria quantum processor, made available through the QLab facility at the University of Maryland. We use 16 qubits for our experiments to limit the circuit depth and effects of noise. All quantum circuits, compiled into native gateset, were executed using API access. We provide further details on circuit execution in Supplementary Information Section F. For the vanishing-rate case, we run the encoding, error and decoding circuit over N physical qubits many times. Because we needed to perform tomography on the single logical qubit, we appended an appropriate basis change Pauli

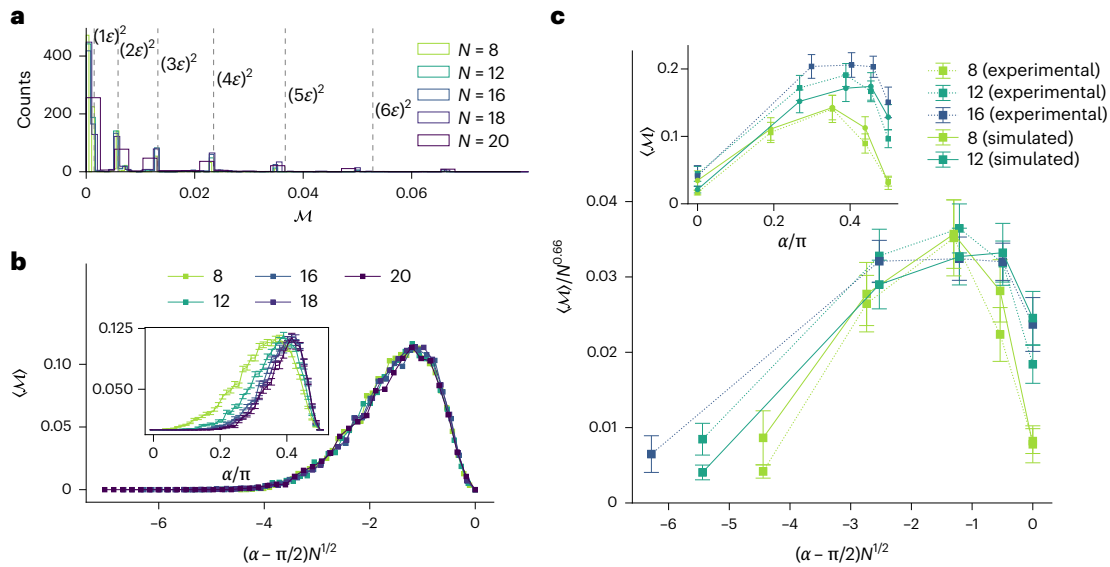


Fig. 2 | Results for vanishing-rate codes. **a**, Distribution of SSRE across codes and syndromes in classical simulation. The distribution is tightly peaked around square-integer multiples of the distance $\epsilon = \pi/2 - \alpha$ from the Clifford point, because it is controlled by the weights of the errors. **b, c**, Syndrome- and circuit-averaged SSRE from classical numerical calculations (**b**) and experimental results on IonQ Aria trapped-ion quantum computer (**c**). Both display the predicted square-root scaling. The error estimates for experiments are derived using bootstrapping (details in Supplementary Information Section H). The scaling with respect to system size of the vertical axis of **c** (main) is chosen to match the

scaling of the peak in unscaled experimental data (inset). For **b**, we plot the mean (with the standard error in the inset) for 1,000 realizations of random circuits for $N = 8, 12, 16$ and 18 , and 500 realizations for $N = 20$. The error bars are omitted in the collapse (main plot). In **c**, we also present numerical data from noisy simulations (solid lines), obtained using a noise model that uses overrotation and depolarizing noise (see Supplementary Information Section K for more details). The data points in **c** present mean with bootstrap error (for experimental points only) over 49 realizations of random circuits for $N = 8$ and 12 , and over 29 realizations for $N = 16$.

gate for each instance of random encoding circuit. Finally, we measured the entire register. Postselecting on syndrome outcomes is prohibitively expensive, so we used the fact that the number of effective actions on the logical qubit (up to a global phase) is much smaller than the number of possible syndromes. This allowed us to group the syndrome into equivalence classes, where elements in a class have the same effective action on the logical qubits. These classes are identified by grouping the rotations using classical simulations. To mitigate incoherent errors, we projected the density matrix of the logical qubit, obtained using tomography of a syndrome class, to its maximum-eigenvalue eigenstate in postprocessing. We then calculate the circuit- and syndrome-averaged magic $\mathcal{M}(\alpha) = \langle |\bar{s}| \times \langle M_{C,\bar{s}} \rangle_{\bar{s} \in \mathcal{S}} \rangle_{C'}$, where \bar{s} denotes syndrome classes and $|\bar{s}|$ denotes the size of a syndrome class \bar{s} .

We present our experimental measurements in Fig. 2c for $N = 8, 12$ and 16 , using 50, 50 and 30 instances, respectively, of random circuits. The error bars are obtained by means of bootstrap resampling (details in Supplementary Information Section H). We observed that, following the mitigation techniques discussed above, we could achieve a measurement of magic that qualitatively resembles the theoretical expectations.

Constant rate

At finite rate—that is, when the number of logical qubits K scales as $K = rN$ with the number of physical qubits N —the finite-magic critical region displayed by the vanishing-rate code becomes an extended magical phase. This magical phase is visible in Fig. 1c, which shows the phase diagram of SSRE as a function of the code and error rate in classical simulations for systems of $N \leq 14$ physical qubits. Figure 3a shows the density of SSRE at fixed rate $r = 1/2$ as a function of error rate α , again in classical simulations. We performed a free-parameter scaling collapse in the linear regime around the crossover, and found that $S/K^\nu \propto (\alpha/\pi - \alpha_c/\pi)^{1/\nu}$ with $\alpha_c = 0.27(1)$, $\nu = 1.15(4)$ and $\gamma = 1.20(8)$. The precise values of the exponents are somewhat sensitive to the size of the regime in which we performed the collapse. Moreover, free-parameter scaling suggests that the magic scales at the critical point

as $N^{1.2}$. But physical intuition suggests that, because the scaling dimension is zero below the critical point and one above the critical point, the scaling dimension at the critical point should be within $[0, 1]$. In Supplementary Information Section M, we present Fig. 3a but with γ constrained to $[0, 1]$.

The scaling collapse indicates that the transition from non-magical to magical is indeed a phase transition, not a crossover.

As the SSRE is an expensive quantity to measure for finite-rate codes, we used the conditional entropy of the logical state as a diagnostic for the phases. In Fig. 3b (upper), we show the phase diagram for conditional entropy density as a function of code rate and error rate. The conditional entropy, without any minimization over basis, serves as an upper bound to the basis-minimized conditional entropy, which is a genuine measure of magic. Moreover, for small α , we have a priori reason to believe that the computational basis is the minimum-entropy basis: the logical state begins in a computational basis state, and when the α is small, it is weakly perturbed, so it remains closer to the computational basis state than any other stabilizer state. This is no longer true at the Clifford point $\alpha = \pi/2$. There the minimum-entropy basis is no longer the computational basis, but some other stabilizer basis; in that basis, the measurement entropy is zero, but in the computational basis, the measurement entropy is extensive. We discuss the relationship between measurement entropy, error correction and decoder breakdown in Supplementary Information Section C.

In Fig. 3c, we present finite-rate scaling, obtained through simulations, of the conditional entropy at code rate $r = 1/2$. For each data point in numerical simulations of sizes $N = 12, 16, 20$ and 24 , we simulated 5,000, 5,000, 500 and 50 circuits, respectively. The procedure used to extract the critical parameters and their errors is described in Supplementary Information Section G. We observed that this critical error rate α_c and critical exponent ν both differ from the SSRE. Given the limited understanding of this model's phases, compounded by the challenges with numerical studies of large systems, it is difficult to have confident estimates of the critical point and exponent. In particular,

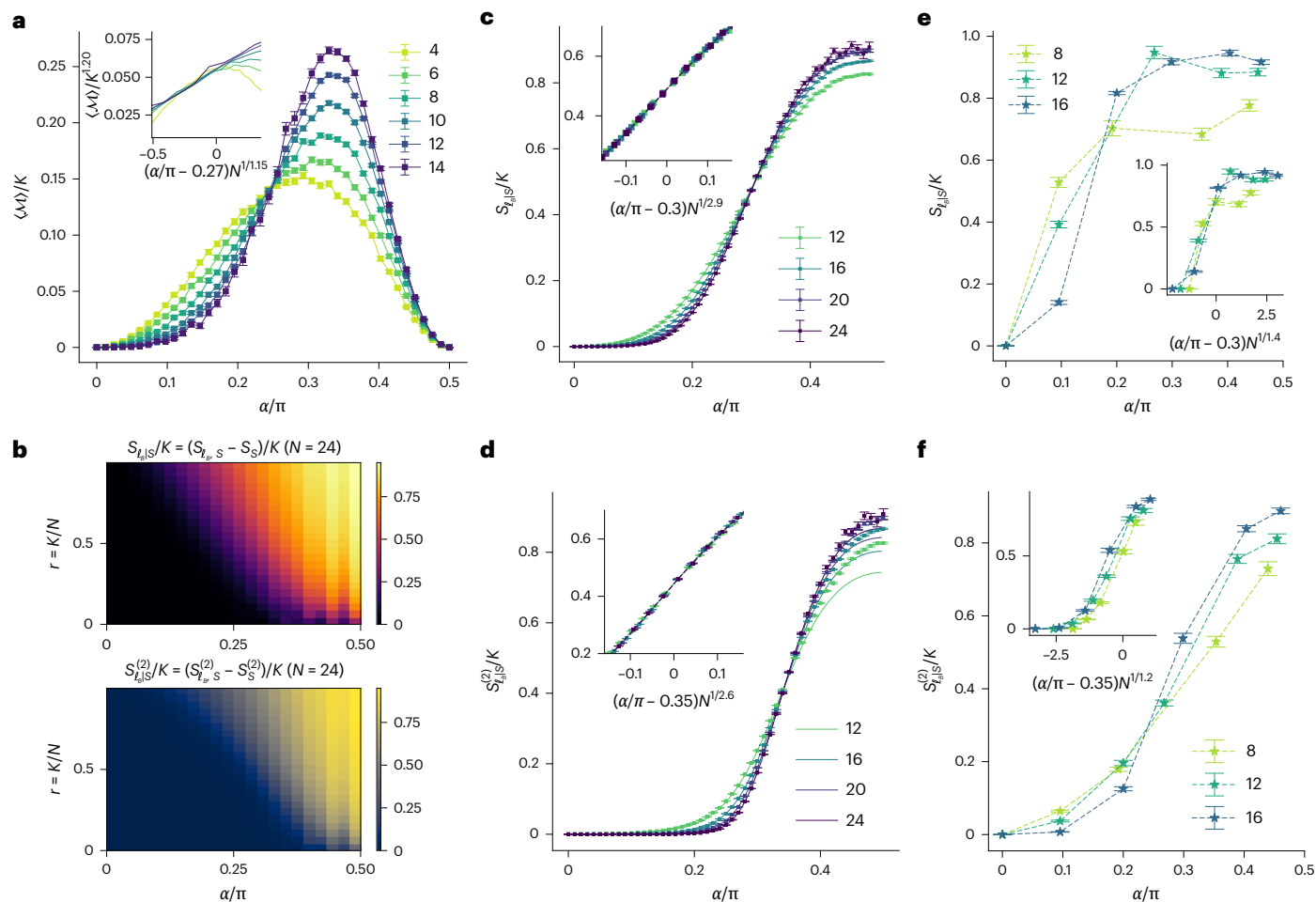


Fig. 3 | Results for constant-rate codes. **a**, Density of magic (SSRE) of the logical space and its scaling collapse (inset) plotted against the error rate α , for code rate $r = K/N = 1/2$, for 1,000 realizations of random circuits for $N \leq 12$ and 200 realizations for $N = 14$. The error bars are derived using standard error and are omitted in the scaling collapse (inset), where the x axis is scaled as $(\alpha/\pi - \alpha_c/\pi)N^{1/\nu}$ with critical parameters $\alpha_c/\pi = 27(1)$ and $\nu = 1.15(4)$, and the y axis is scaled as $\langle \mathcal{M} \rangle / K^\nu$ with $\nu = 1.20(8)$. **b**, Phase diagrams of conditional entropy (upper) and its Rényi approximation (lower), without any basis minimization. **c**, Finite-size scaling of the conditional entropy and its collapse (inset) computed numerically using simulations at $r = 1/2$. The scaling collapse (inset) has critical parameters $\alpha_c/\pi = 0.304(2)$ and $\nu = 2.9(2)$. The data points represent mean and standard error (omitted in the inset) over realizations of 5,000, 5,000, 500 and 50 circuits for $N = 12, 16, 20$ and 24 , respectively. **d**, Finite-size scaling of the Rényi approximation of the conditional entropy and its collapse (inset) computed

numerically using simulations (displayed points) and analytics (solid line) at $r = 1/2$. The scaling collapse, computed with data from simulations, has critical parameters $\alpha_c/\pi = 0.347(1)$ and $\nu = 2.6(2)$. The data points represent mean and standard error (omitted in the inset) over realizations of 5,000, 5,000, 500 and 50 circuits for $N = 12, 16, 20$ and 24 , respectively. **e**, Finite-size scaling of the conditional entropy using data from experiments in IonQ Aria at $r = 1/2$. The data points represent mean with error bars obtained using bootstrap resampling, computed over 49 realizations of random circuits for $N = 8, 12$ and 29 realizations for $N = 16$. The scaling collapse (inset) uses critical exponents derived from numerical simulations of circuits with $d = N/2$, as shown in Supplementary Fig. 2. **f**, Finite-size scaling of the Rényi approximation of the conditional entropy and its collapse (inset) computed using experiments at $r = 1/2$. The data points represent mean with error bars obtained using bootstrap resampling, computed over 49 realizations of random circuits for $N = 8, 12$ and 29 realizations for $N = 16$.

we cannot conclude whether or not the transition point coincides with that of the SSRE, as this depends drastically on the choice of scaling hypothesis. This discussion is left as an outlook. Indeed, our work aims not to unify these diagnostics or resolve their detailed phase transitions but rather to present a transition on non-stabilizerness or magic in the first place.

Analytical calculations

We also observe that the Rényi conditional measurement entropy, the Rényi analogue of the Shannon conditional measurement entropy, exhibits similar phases, as shown in Fig. 3b (lower). The circuit-averaged conditional Rényi entropy is defined as

$$\mathbb{E}_C \left[-\log \sum_{x \in \{0,1\}^N} (p_{(\ell,s)}^{\alpha,C}(x))^2 + \log \sum_{x \in \{0,1\}^{N-K}} (p_s^{\alpha,C}(x))^2 \right], \quad (1)$$

where $p_s^{\alpha,C}(x)$ denotes the probability of measuring x in the syndrome register s , for a state produced with a Clifford encoder C and coherent rotations of strength α . Similarly the (ℓ, s) subscript denotes measurement in the joint syndrome and logical register. For large systems, we can use a typicality argument to assume that the circuit-to-circuit variation in distribution of measurement outcomes is negligible; this allows us to interchange logarithm with expectation over C in equation (1). Finally, we can calculate $\mathbb{E}_C \sum_x (p_s^{\alpha,C}(x))^2$ using Clifford averaging by means of Schur–Weyl duality (see Supplementary Information Section I for details).

Figure 3d shows the finite-size scaling for Rényi conditional measurement entropy for system sizes $N \leq 24$ comparable to those used in classical simulation and experiment, at code rate $r = 1/2$. The analytical result is plotted as solid lines. The data points represent circuit averages computed by means of numerical simulations. For each data point in numerical simulations of sizes $N = 12, 16, 20$ and 24 , we simulated

5,000, 5,000, 500 and 50 circuits, respectively. Indeed, the analytical computation matches the exact numerical data for large systems for which the typicality assumption is true. Although our analytics lets us access arbitrarily large sizes for this observable, we performed the scaling collapse over sizes that are experimentally accessible. The procedure used to perform the scaling collapse and extract related errors is described in Supplementary Section G.

Experiment

The random Clifford code was implemented on up to 16 qubits of IonQ's 32-qubit Aria device. (The implementation was limited not by the number of qubits available but by circuit depth, which, in turn, was limited by gate noise.) The SSRE is not accessible in experiments on finite-rate codes, because it requires full state tomography. The conditional measurement entropy, by contrast, requires only computational basis measurements. These computational basis measurements undergo postprocessing similar to linear cross-entropy benchmarking in random circuit sampling experiments³², using information from classical simulation. The reported entropies are $S_X = -\sum_x p(x) \log \tilde{p}(x)$, where $\tilde{p}(x)$ is the probability anticipated from classical simulation, and $p(x)$ are experimentally obtained distributions projected onto the support of the ideal distribution $\tilde{p}(x)$.

Figure 3e,f show the resulting Shannon and Rényi entropies, respectively. As expected, the scaling of the entropies with respect to system size is inverted across the threshold. Recall that the experiments were performed using circuits of depth $d = N/2$. The scaling collapse (insets) in the experimental data use the critical parameters derived from numerical simulations for $d = N/2$ circuits, as shown in Supplementary Fig. 2b,c in Supplementary Information Section F. For each experimental data point of sizes $N = 8, 12$ and 16 , we executed 50, 50 and 20 different circuit instances, respectively. The error bars were estimated using bootstrap resampling, discussed in Supplementary Information Section H.

Discussion

We have observed that a random Clifford code subject to coherent errors displays a phase transition in magic. Concentrating magic of a large system to a smaller subsystem can be difficult, as has also been shown in ref. 33. In our model, measuring the syndromes of a random Clifford code concentrates magic in the logical space if the error rate or the code rate is above a critical value, and suppresses magic below the threshold. This result establishes a connection between the resource theory of stabilizer computation, that is, magic, and the study of decoder breakdown in quantum error correction codes by means of the basis-minimized measurement entropy.

In this work, we studied phases of magic for small systems for which calculating measures of magic is tractable. In general, non-stabilizerness is difficult to measure. Measures of magic usually require exponentially many measurement samples and often need extensive classical processing, making them intractable for large systems. Our work, however, suggests the possibility of diagnostics, such as the conditional entropy, that can be estimated efficiently using a small number of samples and classical postprocessing. In the future, such measures can be used to study the phase transition in larger systems to better approximate the thermodynamic limit.

Phase transitions in magic—both ours and the theoretical predictions of ref. 33—indicate that existing measurement-induced phase transitions sit in a broader landscape of information-theoretic phase transitions. In each case, the phase transition arises from the competition between three channels—a channel that generates the resource (whether entanglement or magic), a channel that generates correlations and a channel that destroys the resource—that fail to commute. In the phase transition shown here, the correlation-generating channels are the encoding Clifford operations, the resource-generating channels are the rotations $R_x(\alpha)$ of the noise layer and the resource-destroying

maps are syndrome measurements. In the phase transition of ref. 33, the correlation-generating channels are layers of random Clifford gates, the resource-generating channels are interspersed T gates and the resource-destroying maps are partial traces. In the measurement-only entanglement phase transition of ref. 34, all channels are projective measurements: non-local projective measurements generate entanglement as well as correlation, whereas onsite measurements destroy the resource. We conjecture that any information-theoretic setting with this structure of three competing channels can be made to show a phase transition. A related question concerns the nature of universality in these information-theoretic transitions at their critical points. It is currently unclear whether the magic phase transitions studied are indeed part of a universality class of critical phenomena.

Our result also suggests that error correction together with sufficiently well-characterized coherent noise can create useful magic states. In the magical phase, the syndrome measurements move magic from the physical qubits, where non-Clifford gates such as single-qubit rotations are easy, to the logical qubits, where non-Clifford gates are typically hard. Syndrome-dependent Clifford unitaries may then transform these states into states suitable as inputs to existing magic state distillation protocols. In this case, an outstanding challenge is the decoding problem of identifying the right Clifford unitary given a code and a syndrome. Notably, such unitaries are efficiently computable under a wide range of circumstances for zero-rate topological surface codes³⁰. If this can be done more generally, then the magical phase may improve the efficiency of magic state distillation, thereby reducing overhead in quantum computation algorithms where magic state distillation is the bottleneck.

Online content

Any methods, additional references, Nature Portfolio reporting summaries, source data, extended data, supplementary information, acknowledgements, peer review information; details of author contributions and competing interests; and statements of data and code availability are available at <https://doi.org/10.1038/s41567-024-02637-3>.

References

- Gottesman, D. The Heisenberg representation of quantum computers. Preprint at <https://doi.org/10.48550/arXiv.quant-ph/9807006> (1998).
- Aaronson, S. & Gottesman, D. Improved simulation of stabilizer circuits. *Phys. Rev. A* **70**, 052328 (2004).
- Bravyi, S. et al. Simulation of quantum circuits by low-rank stabilizer decompositions. *Quantum* **3**, 181 (2019).
- Bu, K. & Koh, D. E. Efficient classical simulation of clifford circuits with nonstabilizer input states. *Phys. Rev. Lett.* **123**, 170502 (2019).
- Bravyi, S. & Kitaev, A. Universal quantum computation with ideal Clifford gates and noisy ancillas. *Phys. Rev. A* **71**, 022316 (2005).
- Fowler, A. G., Mariantoni, M., Martinis, J. M. & Cleland, A. N. Surface codes: towards practical large-scale quantum computation. *Phys. Rev. A* **86**, 032324 (2012).
- O’Gorman, J. & Campbell, E. T. Quantum computation with realistic magic-state factories. *Phys. Rev. A* **95**, 032338 (2017).
- Campbell, E. T., Terhal, B. M. & Vuillot, C. Roads towards fault-tolerant universal quantum computation. *Nature* **549**, 172–179 (2017).
- Veitch, V., Mousavian, S. A. H., Gottesman, D. & Emerson, J. The resource theory of stabilizer computation. *New J. Phys.* **16**, 013009 (2014).
- Bu, K., Garcia, R. J., Jaffe, A., Koh, D. E. & Li, L. Complexity of quantum circuits via sensitivity, magic and coherence. *Commun. Math. Phys.* **405**, 161 (2024).
- White, C. D., Cao, C. & Swingle, B. Conformal field theories are magical. *Phys. Rev. B* **103**, 075145 (2021).
- Leone, L., Oliviero, S. F., Zhou, Y. & Hamma, A. Quantum chaos is quantum. *Quantum* **5**, 453 (2021).

13. Skinner, B., Ruhman, J. & Nahum, A. Measurement-induced phase transitions in the dynamics of entanglement. *Phys. Rev. X* **9**, 031009 (2019).
14. Li, Y., Chen, X. & Fisher, M. P. A. Measurement-driven entanglement transition in hybrid quantum circuits. *Phys. Rev. B* **100**, 134306 (2019).
15. Terhal, B. M. Quantum error correction for quantum memories. *Rev. Mod. Phys.* **87**, 307–346 (2015).
16. Potter, A. C. & Vasseur, R. in *Entanglement in Spin Chains: From Theory to Quantum Technology Applications* (eds Bayat, A. et al.) 211–249 (Springer, 2022).
17. Fisher, M. P., Khemani, V., Nahum, A. & Vijay, S. Random quantum circuits. *Ann. Rev. Condens. Matter Phys.* **14**, 335–379 (2023).
18. Zabalo, A. et al. Operator scaling dimensions and multifractality at measurement-induced transitions. *Phys. Rev. Lett.* **128**, 050602 (2022).
19. Iaconis, J., Lucas, A. & Chen, X. Measurement-induced phase transitions in quantum automaton circuits. *Phys. Rev. B* **102**, 224311 (2020).
20. Gullans, M. J. & Huse, D. A. Dynamical purification phase transition induced by quantum measurements. *Phys. Rev. X* **10**, 041020 (2020).
21. Bao, Y., Choi, S. & Altman, E. Theory of the phase transition in random unitary circuits with measurements. *Phys. Rev. B* **101**, 104301 (2020).
22. Jian, C.-M., You, Y.-Z., Vasseur, R. & Ludwig, A. W. W. Measurement-induced criticality in random quantum circuits. *Phys. Rev. B* **101**, 104302 (2020).
23. Li, Y., Vasseur, R., Fisher, M. P. & Ludwig, A. W. Statistical mechanics model for clifford random tensor networks and monitored quantum circuits. *Phys. Rev. B* **109**, 174307 (2024).
24. Barratt, F. et al. Field theory of charge sharpening in symmetric monitored quantum circuits. *Phys. Rev. Lett.* **129**, 120604 (2022).
25. Agrawal, U. et al. Entanglement and charge-sharpening transitions in $U(1)$ symmetric monitored quantum circuits. *Phys. Rev. X* **12**, 041002 (2022).
26. Leone, L., Oliviero, S. F. E. & Hamma, A. Stabilizer Rényi entropy. *Phys. Rev. Lett.* **128**, 050402 (2022).
27. Brown, W. & Fawzi, O. Short random circuits define good quantum error correcting codes. In *2013 IEEE International Symposium on Information Theory* 346–350 (IEEE, 2013).
28. Haug, T. & Piroli, L. Stabilizer entropies and nonstabilizerness monotones. *Quantum* **7**, 1092 (2023).
29. Gottesman, D. *Stabilizer Codes and Quantum Error Correction* (California Institute of Technology, 1997).
30. Bravyi, S., Englbrecht, M., König, R. & Peard, N. Correcting coherent errors with surface codes. *NPJ Quantum Inf.* **4**, 55 (2018).
31. Venn, F., Behrends, J. & Béri, B. Coherent-error threshold for surface codes from Majorana delocalization. *Phys. Rev. Lett.* **131**, 060603 (2023).
32. Arute, F. et al. Quantum supremacy using a programmable superconducting processor. *Nature* **574**, 505–510 (2019).
33. Leone, L., Oliviero, S. F., Esposito, G. & Hamma, A. Phase transition in stabilizer entropy and efficient purity estimation. *Phys. Rev. A* **109**, 032403 (2024).
34. Ippoliti, M., Gullans, M. J., Gopalakrishnan, S., Huse, D. A. & Khemani, V. Entanglement phase transitions in measurement-only dynamics. *Phys. Rev. X* **11**, 011030 (2021).
35. Pradeep, N. et al. Phase transition in magic with random quantum circuits. *Zenodo* <https://doi.org/10.5281/zenodo.7847794> (2024).

Publisher's note Springer Nature remains neutral with regard to jurisdictional claims in published maps and institutional affiliations.

Springer Nature or its licensor (e.g. a society or other partner) holds exclusive rights to this article under a publishing agreement with the author(s) or other rightsholder(s); author self-archiving of the accepted manuscript version of this article is solely governed by the terms of such publishing agreement and applicable law.

© The Author(s), under exclusive licence to Springer Nature Limited 2024

Data availability

All the data used in this work can be found via Zenodo at <https://doi.org/10.5281/zenodo.7847794> (ref. 35). Source data are provided with this paper.

Acknowledgements

We thank K. Wright, M. Hiles and J. Nguyen from IonQ for their assistance, and L. Zhukas, N. Yunger Halpern, W. Braasch and B. Ware for comments on the manuscript. We are also grateful to an anonymous reviewer for a thorough, careful and thoughtful review. This work is supported by the NSF STAQ program; the NSF QLCI RQS Program OMA-2120757; the DOE QSA program DE-FOA-0002253; and the AFOSR MURIs on Dissipation Engineering in Open Quantum Systems, Quantum Measurement/Verification, and Quantum Interactive Protocols. C.D.W. thanks DOE-ASCR Quantum Computing Application Teams program for support under fieldwork proposal number ERKJ347. The experiments were performed on the IonQ Aria system through the UMD/IonQ Q-Lab consortium. Certain commercial equipment, instruments or materials are identified in this paper in order to specify the experimental procedure adequately. Such identification is not intended to imply recommendation or endorsement by the National Institute of Standards and Technology, nor is it intended to imply that the materials or equipment identified are necessarily the best available for the purpose.

Author contributions

P.N., C.D.W. and M.J.G. developed the theory. P.N. collected and analysed the data. Q.W., S.J., D.Z. and C.N. provided support and guidance on experiments. C.M., C.N. and M.J.G. supervised the project. All authors discussed results and contributed to the manuscript.

Competing interests

The authors declare no competing interests.

Additional information

Supplementary information The online version contains supplementary material available at <https://doi.org/10.1038/s41567-024-02637-3>.

Correspondence and requests for materials should be addressed to Pradeep Niroula or Michael J. Gullans.

Peer review information *Nature Physics* thanks Alioscia Hama, Xhek Turkeshi and Guo-Yi Zhu for their contribution to the peer review of this work.

Reprints and permissions information is available at www.nature.com/reprints.